Research Article | Vol. 9, No. 8 | 1 Aug 2018 | BIOMEDICAL OPTICS EXPRESS 3653
Biomedical Optics EXPRESS

Noninvasive *in vivo* characterization of erythrocyte motion in human retinal capillaries using high-speed adaptive optics near-confocal imaging

Boyu Gu,[1] Xiaolin Wang,[1] Michael D. Twa,[2] Johnny Tam,[3] Christopher A. Girkin,[1] and Yuhua Zhang[1,*]

[1]*Department of Ophthalmology and Visual Sciences, School of Medicine, University of Alabama at Birmingham, 1670 University Boulevard, Birmingham, AL 35294, USA*
[2]*Department of Optometry and Vision Science, School of Optometry, University of Alabama at Birmingham, 1716 University Boulevard, Birmingham, AL 35294, USA*
[3]*National Eye Institute, National Institutes of Health, 10 Center Drive, Bethesda, MD 20892, USA*
**yuhuazhang@uabmc.edu*

Abstract: The flow of erythrocytes in parafoveal capillaries was imaged in the living human eye with an adaptive optics near-confocal ophthalmoscope at a frame rate of 800 Hz with a low coherence near-infrared (NIR) light source. Spatiotemporal traces of the erythrocyte movement were extracted from consecutive images. Erythrocyte velocity was measured using custom software based on the Radon transform. The impact of imaging speed on velocity measurement was estimated using images of frame rates of 200, 400, and 800 Hz. The NIR light allowed for long imaging periods without visually stimulating the retina and disturbing the natural rheological state. High speed near-confocal imaging enabled direct and accurate measurement of erythrocyte velocity, and revealed a distinctively cardiac-dependent pulsatile velocity waveform of the erythrocyte flow in retinal capillaries, disclosed the impact of the leukocytes on erythrocyte motion, and provided new metrics for precise assessment of erythrocyte movement. The approach may facilitate new investigations on the pathophysiology of retinal microcirculation with applications for ocular and systemic diseases.

OCIS codes: (170.4460) Ophthalmic optics and devices; (330.4300) Vision system - noninvasive assessment; (120.3890) Medical optics instrumentation; (170.0110) Imaging systems; (220.1080) Active or adaptive optics.

References and links

1. M. T. Wong-Riley, "Energy metabolism of the visual system," Eye Brain **2**, 99–116 (2010).
2. C. J. Pournaras, E. Rungger-Brändle, C. E. Riva, S. H. Hardarson, and E. Stefansson, "Regulation of retinal blood flow in health and disease," Prog. Retin. Eye Res. **27**(3), 284–330 (2008).
3. D. Attwell, A. M. Buchan, S. Charpak, M. Lauritzen, B. A. Macvicar, and E. A. Newman, "Glial and neuronal control of brain blood flow," Nature **468**(7321), 232–243 (2010).
4. D. A. Antonetti, R. Klein, and T. W. Gardner, "Diabetic retinopathy," N. Engl. J. Med. **366**(13), 1227–1239 (2012).
5. M. Emre, S. Orgül, K. Gugleta, and J. Flammer, "Ocular blood flow alteration in glaucoma is related to systemic vascular dysregulation," Br. J. Ophthalmol. **88**(5), 662–666 (2004).
6. Z. Burgansky-Eliash, H. Barash, D. Nelson, A. Grinvald, A. Sorkin, A. Loewenstein, and A. Barak, "Retinal blood flow velocity in patients with age-related macular degeneration," Curr. Eye Res. **39**(3), 304–311 (2014).
7. M. Ritt, J. M. Harazny, C. Ott, U. Raff, P. Bauernschubert, M. Lehmann, G. Michelson, and R. E. Schmieder, "Impaired increase of retinal capillary blood flow to flicker light exposure in arterial hypertension," Hypertension **60**(3), 871–876 (2012).
8. N. Patton, T. Aslam, T. Macgillivray, A. Pattie, I. J. Deary, and B. Dhillon, "Retinal vascular image analysis as a potential screening tool for cerebrovascular disease: a rationale based on homology between cerebral and retinal microvasculatures," J. Anat. **206**(4), 319–348 (2005).
9. M. L. Baker, P. J. Hand, J. J. Wang, and T. Y. Wong, "Retinal signs and stroke: revisiting the link between the eye and brain," Stroke **39**(4), 1371–1379 (2008).

#331585 https://doi.org/10.1364/BOE.9.003653
Journal © 2018 Received 15 May 2018; revised 2 Jul 2018; accepted 2 Jul 2018; published 12 Jul 2018

Biomedical Optics EXPRESS

10. F. Berisha, G. T. Feke, C. L. Trempe, J. W. McMeel, and C. L. Schepens, "Retinal abnormalities in early Alzheimer's disease," Invest. Ophthalmol. Vis. Sci. **48**(5), 2285–2289 (2007).
11. G. T. Feke, B. T. Hyman, R. A. Stern, and L. R. Pasquale, "Retinal blood flow in mild cognitive impairment and Alzheimer's disease," Alzheimers Dement (Amst) **1**(2), 144–151 (2015).
12. C. J. Pournaras and C. E. Riva, "Retinal blood flow evaluation," Ophthalmologica **229**(2), 61–74 (2013).
13. G. T. Feke and C. E. Riva, "Laser Doppler measurements of blood velocity in human retinal vessels," J. Opt. Soc. Am. **68**(4), 526–531 (1978).
14. B. L. Petrig and C. E. Riva, "Near-IR retinal laser Doppler velocimetry and flowmetry: new delivery and detection techniques," Appl. Opt. **30**(16), 2073–2078 (1991).
15. B. White, M. Pierce, N. Nassif, B. Cense, B. Park, G. Tearney, B. Bouma, T. Chen, and J. de Boer, "*In vivo* dynamic human retinal blood flow imaging using ultra-high-speed spectral domain optical coherence tomography," Opt. Express **11**(25), 3490–3497 (2003).
16. W. Choi, B. Baumann, J. J. Liu, A. C. Clermont, E. P. Feener, J. S. Duker, and J. G. Fujimoto, "Measurement of pulsatile total blood flow in the human and rat retina with ultrahigh speed spectral/Fourier domain OCT," Biomed. Opt. Express **3**(5), 1047–1061 (2012).
17. A. I. Srienc, Z. L. Kurth-Nelson, and E. A. Newman, "Imaging retinal blood flow with laser speckle flowmetry," Front. Neuroenergetics **2010**, 2 (2010).
18. T. Sugiyama, M. Araie, C. E. Riva, L. Schmetterer, and S. Orgul, "Use of laser speckle flowgraphy in ocular blood flow research," Acta Ophthalmol. **88**(7), 723–729 (2010).
19. C. Dai, X. Liu, H. F. Zhang, C. A. Puliafito, and S. Jiao, "Absolute retinal blood flow measurement with a dual-beam Doppler optical coherence tomography," Invest. Ophthalmol. Vis. Sci. **54**(13), 7998–8003 (2013).
20. R. A. Leitgeb, R. M. Werkmeister, C. Blatter, and L. Schmetterer, "Doppler optical coherence tomography," Prog. Retin. Eye Res. **41**, 26–43 (2014).
21. D. Izhaky, D. A. Nelson, Z. Burgansky-Eliash, and A. Grinvald, "Functional imaging using the retinal function imager: Direct imaging of blood velocity, achieving fluorescein angiography-like images without any contrast agent, qualitative oximetry, and functional metabolic signals," Jpn. J. Ophthalmol. **53**(4), 345–351 (2009).
22. L. Wang, H. Jiang, A. Grinvald, C. Jayadev, and J. Wang, "A mini review of clinical and research applications of the retinal function imager," Curr. Eye Res. **43**(3), 273–288 (2018).
23. Q. Wang, O. P. Kocaoglu, B. Cense, J. Bruestle, R. S. Jonnal, W. Gao, and D. T. Miller, "Imaging retinal capillaries using ultrahigh-resolution optical coherence tomography and adaptive optics," Invest. Ophthalmol. Vis. Sci. **52**(9), 6292–6299 (2011).
24. M. Meinke, G. Müller, J. Helfmann, and M. Friebel, "Optical properties of platelets and blood plasma and their influence on the optical behavior of whole blood in the visible to near infrared wavelength range," J. Biomed. Opt. **12**(1), 014024 (2007).
25. R. Flower, E. Peiretti, M. Magnani, L. Rossi, S. Serafini, Z. Gryczynski, and I. Gryczynski, "Observation of erythrocyte dynamics in the retinal capillaries and choriocapillaris using ICG-loaded erythrocyte ghost cells," Invest. Ophthalmol. Vis. Sci. **49**(12), 5510–5516 (2008).
26. T. E. Kornfield and E. A. Newman, "Regulation of blood flow in the retinal trilaminar vascular network," J. Neurosci. **34**(34), 11504–11513 (2014).
27. T. E. Kornfield and E. A. Newman, "Measurement of retinal blood flow using fluorescently labeled red blood cells," eNeuro **2**(2), 0005–0015 (2015).
28. A. Guevara-Torres, A. Joseph, and J. B. Schallek, "Label free measurement of retinal blood cell flux, velocity, hematocrit and capillary width in the living mouse eye," Biomed. Opt. Express **7**(10), 4228–4249 (2016).
29. G. Richard, G. Soubrane, and L. Yanuzzi, *Fluorescein Angiography: Textbook and Atlas,* 2nd ed. (Thieme Medical Publishes Inc., New York, 1998).
30. A. N. S. Institute, "American National Standard for Safe Use of Lasers ANSI Z136.1-2014," (American National Standards Institute, Inc., 2014).
31. A. Roorda and J. L. Duncan, "Adaptive optics ophthalmoscopy," Annu Rev Vis Sci **1**(1), 19–50 (2015).
32. S. Marcos, J. S. Werner, S. A. Burns, W. H. Merigan, P. Artal, D. A. Atchison, K. M. Hampson, R. Legras, L. Lundstrom, G. Yoon, J. Carroll, S. S. Choi, N. Doble, A. M. Dubis, A. Dubra, A. Elsner, R. Jonnal, D. T. Miller, M. Paques, H. E. Smithson, L. K. Young, Y. Zhang, M. Campbell, J. Hunter, A. Metha, G. Palczewska, J. Schallek, and L. C. Sincich, "Vision science and adaptive optics, the state of the field," Vision Res. **132**, 3–33 (2017).
33. M. Pircher and R. J. Zawadzki, "Review of adaptive optics OCT (AO-OCT): principles and applications for retinal imaging [Invited]," Biomed. Opt. Express **8**(5), 2536–2562 (2017).
34. J. Liang, D. R. Williams, and D. T. Miller, "Supernormal vision and high-resolution retinal imaging through adaptive optics," J. Opt. Soc. Am. A **14**(11), 2884–2892 (1997).
35. A. Roorda, F. Romero-Borja, W. Donnelly Iii, H. Queener, T. Hebert, and M. Campbell, "Adaptive optics scanning laser ophthalmoscopy," Opt. Express **10**(9), 405–412 (2002).
36. J. A. Martin and A. Roorda, "Pulsatility of parafoveal capillary leukocytes," Exp. Eye Res. **88**(3), 356–360 (2009).
37. J. A. Martin and A. Roorda, "Direct and noninvasive assessment of parafoveal capillary leukocyte velocity," Ophthalmology **112**(12), 2219–2224 (2005).

Biomedical Optics EXPRESS

38. J. Tam, P. Tiruveedhula, and A. Roorda, "Characterization of single-file flow through human retinal parafoveal capillaries using an adaptive optics scanning laser ophthalmoscope," Biomed. Opt. Express **2**(4), 781–793 (2011).
39. J. Tam and A. Roorda, "Speed quantification and tracking of moving objects in adaptive optics scanning laser ophthalmoscopy," J. Biomed. Opt. **16**(3), 036002 (2011).
40. A. Uji, M. Hangai, S. Ooto, K. Takayama, N. Arakawa, H. Imamura, K. Nozato, and N. Yoshimura, "The source of moving particles in parafoveal capillaries detected by adaptive optics scanning laser ophthalmoscopy," Invest. Ophthalmol. Vis. Sci. **53**(1), 171–178 (2012).
41. S. Arichika, A. Uji, M. Hangai, S. Ooto, and N. Yoshimura, "Noninvasive and direct monitoring of erythrocyte aggregates in human retinal microvasculature using adaptive optics scanning laser ophthalmoscopy," Invest. Ophthalmol. Vis. Sci. **54**(6), 4394–4402 (2013).
42. S. Arichika, A. Uji, S. Ooto, K. Miyamoto, and N. Yoshimura, "Adaptive optics-assisted identification of preferential erythrocyte aggregate pathways in the human retinal microvasculature," PLoS One **9**(2), e89679 (2014).
43. S. Arichika, A. Uji, T. Murakami, N. Unoki, S. Yoshitake, Y. Dodo, S. Ooto, K. Miyamoto, and N. Yoshimura, "Retinal hemorheologic characterization of early-stage diabetic retinopathy using adaptive optics scanning laser ophthalmoscopy," Invest. Ophthalmol. Vis. Sci. **55**(12), 8513–8522 (2014).
44. Z. Zhong, B. L. Petrig, X. Qi, and S. A. Burns, "*In vivo* measurement of erythrocyte velocity and retinal blood flow using adaptive optics scanning laser ophthalmoscopy," Opt. Express **16**(17), 12746–12756 (2008).
45. Z. Zhong, H. Song, T. Y. Chui, B. L. Petrig, and S. A. Burns, "Noninvasive measurements and analysis of blood velocity profiles in human retinal vessels," Invest. Ophthalmol. Vis. Sci. **52**(7), 4151–4157 (2011).
46. A. de Castro, G. Huang, L. Sawides, T. Luo, and S. A. Burns, "Rapid high resolution imaging with a dual-channel scanning technique," Opt. Lett. **41**(8), 1881–1884 (2016).
47. Y. Lu, M. O. Bernabeu, J. Lammer, C. C. Cai, M. L. Jones, C. A. Franco, L. P. Aiello, and J. K. Sun, "Computational fluid dynamics assisted characterization of parafoveal hemodynamics in normal and diabetic eyes using adaptive optics scanning laser ophthalmoscopy," Biomed. Opt. Express **7**(12), 4958–4973 (2016).
48. Y. Iida, T. Akagi, H. Nakanishi, H. Ohashi Ikeda, S. Morooka, K. Suda, T. Hasegawa, S. Yokota, M. Yoshikawa, A. Uji, and N. Yoshimura, "Retinal Blood Flow Velocity Change in Parafoveal Capillary after Topical Tafluprost Treatment in Eyes with Primary Open-angle Glaucoma," Sci. Rep. **7**(1), 5019 (2017).
49. M. L. Ellsworth, C. G. Ellis, D. Goldman, A. H. Stephenson, H. H. Dietrich, and R. S. Sprague, "Erythrocytes: oxygen sensors and modulators of vascular tone," Physiology (Bethesda) **24**(2), 107–116 (2009).
50. R. S. Sprague and M. L. Ellsworth, "Erythrocyte-derived ATP and perfusion distribution: role of intracellular and intercellular communication," Microcirculation **19**(5), 430–439 (2012).
51. H. S. Wei, H. Kang, I. D. Rasheed, S. Zhou, N. Lou, A. Gershteyn, E. D. McConnell, Y. Wang, K. E. Richardson, A. F. Palmer, C. Xu, J. Wan, and M. Nedergaard, "Erythrocytes Are Oxygen-Sensing Regulators of the Cerebral Microcirculation," Neuron **91**(4), 851–862 (2016).
52. T. Y. Chui, D. A. Vannasdale, and S. A. Burns, "The use of forward scatter to improve retinal vascular imaging with an adaptive optics scanning laser ophthalmoscope," Biomed. Opt. Express **3**(10), 2537–2549 (2012).
53. P. Bedggood and A. Metha, "Direct visualization and characterization of erythrocyte flow in human retinal capillaries," Biomed. Opt. Express **3**(12), 3264–3277 (2012).
54. P. Bedggood and A. Metha, "Analysis of contrast and motion signals generated by human blood constituents in capillary flow," Opt. Lett. **39**(3), 610–613 (2014).
55. J. Lu, B. Gu, X. Wang, and Y. Zhang, "Adaptive optics parallel near-confocal scanning ophthalmoscopy," Opt. Lett. **41**(16), 3852–3855 (2016).
56. J. Lu, B. Gu, X. Wang, and Y. Zhang, "High speed adaptive optics ophthalmoscopy with an anamorphic point spread function," Opt. Express **26**(11), 14356–14374 (2018).
57. S. Yuan and J. Sasian, "Aberrations of anamorphic optical systems. I: The first-order foundation and method for deriving the anamorphic primary aberration coefficients," Appl. Opt. **48**(13), 2574–2584 (2009).
58. S. Yuan and J. Sasian, "Aberrations of anamorphic optical systems. II. Primary aberration theory for cylindrical anamorphic systems," Appl. Opt. **48**(15), 2836–2841 (2009).
59. J. B. Pawley, "Points, pixels, and gray levels: digitizing image data," in *Handbook of Biological Confocal Microscopy* (Springer, 2006), pp. 59–79.
60. A. Meadway, C. A. Girkin, and Y. Zhang, "A dual-modal retinal imaging system with adaptive optics," Opt. Express **21**(24), 29792–29807 (2013).
61. A. Meadway, X. Wang, C. A. Curcio, and Y. Zhang, "Microstructure of subretinal drusenoid deposits revealed by adaptive optics imaging," Biomed. Opt. Express **5**(3), 713–727 (2014).
62. Y. Yu, T. Zhang, A. Meadway, X. Wang, and Y. Zhang, "High-speed adaptive optics for imaging of the living human eye," Opt. Express **23**(18), 23035–23052 (2015).
63. Y. Yu and Y. Zhang, "Dual-thread parallel control strategy for ophthalmic adaptive optics," Chin. Opt. Lett. **12**(12), 121202 (2014).
64. F. C. Delori, R. H. Webb, and D. H. Sliney; American National Standards Institute, "Maximum permissible exposures for ocular safety (ANSI 2000), with emphasis on ophthalmic devices," J. Opt. Soc. Am. A **24**(5), 1250–1265 (2007).

Biomedical Optics EXPRESS

65. T. Zhang, P. Godara, E. R. Blanco, R. L. Griffin, X. Wang, C. A. Curcio, and Y. Zhang, "Variability in human cone topography assessed by adaptive optics scanning laser ophthalmoscopy," Am. J. Ophthalmol. **160**(2), 290–300 (2015).
66. C. R. Vogel, D. W. Arathorn, A. Roorda, and A. Parker, "Retinal motion estimation in adaptive optics scanning laser ophthalmoscopy," Opt. Express **14**(2), 487–497 (2006).
67. J. Tam and A. Roorda, "Enhanced detection of cell paths in spatiotemporal plots for noninvasive microscopy of the human retina," in *Biomedical Imaging: From Nano to Macro, 2010 IEEE International Symposium on*, (IEEE, 2010), 584–587.
68. D. D. Duncan, P. Lemaillet, M. Ibrahim, Q. D. Nguyen, M. Hiller, and J. Ramella-Roman, "Absolute blood velocity measured with a modified fundus camera," J. Biomed. Opt. **15**(5), 056014 (2010).
69. T. Sugiyama, "Basic Technology and Clinical Applications of the Updated Model of Laser Speckle Flowgraphy to Ocular Diseases," Photonics **1**(3), 220–234 (2014).
70. N. Chapman, N. Witt, X. Gao, A. A. Bharath, A. V. Stanton, S. A. Thom, and A. D. Hughes, "Computer algorithms for the automated measurement of retinal arteriolar diameters," Br. J. Ophthalmol. **85**(1), 74–79 (2001).
71. N. Bosschaart, G. J. Edelman, M. C. Aalders, T. G. van Leeuwen, and D. J. Faber, "A literature review and novel theoretical approach on the optical properties of whole blood," Lasers Med. Sci. **29**(2), 453–479 (2014).
72. M. R. Martins, W. P. Martins, C. A. M. Soares, A. H. Miyague, M. J. Kudla, and T. Z. Pavan, "Understanding the influence of flow velocity, wall motion filter, pulse repetition frequency, and aliasing on power doppler image quantification," J. Ultrasound Med. (2017).
73. G. W. Schmid-Schönbein, Y. Y. Shih, and S. Chien, "Morphometry of human leukocytes," Blood **56**(5), 866–875 (1980).
74. J. J. Hunter, J. I. Morgan, W. H. Merigan, D. H. Sliney, J. R. Sparrow, and D. R. Williams, "The susceptibility of the retina to photochemical damage from visible light," Prog. Retin. Eye Res. **31**(1), 28–42 (2012).
75. J. Lu, B. Gu, X. Wang, and Y. Zhang, "High-speed adaptive optics line scan confocal retinal imaging for human eye," PLoS One **12**(3), e0169358 (2017).
76. Y. Jia, S. T. Bailey, T. S. Hwang, S. M. McClintic, S. S. Gao, M. E. Pennesi, C. J. Flaxel, A. K. Lauer, D. J. Wilson, J. Hornegger, J. G. Fujimoto, and D. Huang, "Quantitative optical coherence tomography angiography of vascular abnormalities in the living human eye," Proc. Natl. Acad. Sci. U.S.A. **112**(18), E2395–E2402 (2015).
77. N. Hussain, A. Hussain, M. Zhang, J. P. Su, G. Liu, T. S. Hwang, S. T. Bailey, and D. Huang, "Optical Coherence Tomography Angiography," Int J Retina Vitreous **2**(OCT), 27–36 (2016).
78. A. Koustenis, Jr., A. Harris, J. Gross, I. Januleviciene, A. Shah, and B. Siesky, "Optical coherence tomography angiography: an overview of the technology and an assessment of applications for clinical research," Br. J. Ophthalmol. **101**(1), 16–20 (2017).
79. M. Ang, A. C. S. Tan, C. M. G. Cheung, P. A. Keane, R. Dolz-Marco, C. C. A. Sng, and L. Schmetterer, "Optical coherence tomography angiography: a review of current and future clinical applications," Graefes Arch. Clin. Exp. Ophthalmol. **256**(2), 237–245 (2018).
80. H. Nishiwaki, Y. Ogura, H. Kimura, J. Kiryu, and Y. Honda, "Quantitative evaluation of leukocyte dynamics in retinal microcirculation," Invest. Ophthalmol. Vis. Sci. **36**(1), 123–130 (1995).
81. K. Fillacier, G. A. Peyman, Q. Luo, and B. Khoobehi, "Study of lymphocyte dynamics in the ocular circulation: technique of labeling cells," Curr. Eye Res. **14**(7), 579–584 (1995).
82. P. S. Jensen and M. R. Glucksberg, "Regional variation in capillary hemodynamics in the cat retina," Invest. Ophthalmol. Vis. Sci. **39**(2), 407–415 (1998).
83. J. Ben-nun, "Comparative flow velocity of erythrocytes and leukocytes in feline retinal capillaries," Invest. Ophthalmol. Vis. Sci. **37**(9), 1854–1859 (1996).
84. C. E. Riva and B. Petrig, "Blue field entoptic phenomenon and blood velocity in the retinal capillaries," J. Opt. Soc. Am. **70**(10), 1234–1238 (1980).
85. A. G. Koutsiaris, S. V. Tachmitzi, P. Papavasileiou, N. Batis, M. G. Kotoula, A. D. Giannoukas, and E. Tsironi, "Blood velocity pulse quantification in the human conjunctival pre-capillary arterioles," Microvasc. Res. **80**(2), 202–208 (2010).
86. H. Wilkens, W. Regelson, and F. S. Hoffmeister, "The physiolgic importance of pulsatile blood flow," N. Engl. J. Med. **267**(9), 443–446 (1962).
87. T. P. Santisakultarm, N. R. Cornelius, N. Nishimura, A. I. Schafer, R. T. Silver, P. C. Doerschuk, W. L. Olbricht, and C. B. Schaffer, "*In vivo* two-photon excited fluorescence microscopy reveals cardiac- and respiration-dependent pulsatile blood flow in cortical blood vessels in mice," Am. J. Physiol. Heart Circ. Physiol. **302**(7), H1367–H1377 (2012).
88. T. N. Kim, P. W. Goodwill, Y. Chen, S. M. Conolly, C. B. Schaffer, D. Liepmann, and R. A. Wang, "Line-scanning particle image velocimetry: an optical approach for quantifying a wide range of blood flow speeds in live animals," PLoS One **7**(6), e38590 (2012).
89. C. Federau, P. Hagmann, P. Maeder, M. Müller, R. Meuli, M. Stuber, and K. O'Brien, "Dependence of brain intravoxel incoherent motion perfusion parameters on the cardiac cycle," PLoS One **8**(8), e72856 (2013).
90. J. T. O'Brien, "Vascular cognitive impairment," Am. J. Geriatr. Psychiatry **14**(9), 724–733 (2006).
91. D. D. Gutterman, D. S. Chabowski, A. O. Kadlec, M. J. Durand, J. K. Freed, K. Ait-Aissa, and A. M. Beyer, "The human microcirculation: regulation of flow and beyond," Circ. Res. **118**(1), 157–172 (2016).

Biomedical Optics EXPRESS

1. Introduction

Microcirculation in retinal capillaries plays a critical role in support of the intense metabolic activities of the inner retinal tissue in the human eye [1]. Controlled by homeostatic mechanisms, the blood flow is dynamically adjusted to meet the biological and physiological requirements of the retinal tissue by the hemodynamic response system [2, 3]. These processes can be disrupted by common eye diseases such as diabetic retinopathy [4], glaucoma [5], age-related macular degeneration [6], and by systemic diseases or central nervous system (CNS) disorders including hypertension [7], stroke [8, 9], and Alzheimer's disease [10, 11]. Thus, accurate assessment of retinal hemodynamics at the capillary level is of particular importance to understanding normal physiologic processes and pathologic conditions in the retina and facilitating novel treatments for retinal diseases.

Optical imaging has been a major method for investigating retinal hemodynamics due to its unique ability to access the retina through the eye's optics [12]. In the past four decades, several techniques have been developed to measure retinal blood flow and velocity [12], but *in vivo* characterization of retinal hemodynamics in the capillaries of the human eye remains challenging due to a number of technical obstacles. First, many established methods, such as laser Doppler velocimetry [13, 14], optical coherence tomography (OCT) [15, 16], laser speckle imaging [17, 18], Doppler OCT [19, 20], and the Retinal Functional Imager based upon rapid sequential imaging [21, 22], do not possess the spatial resolution required for imaging the retinal capillary (~5 μm) [23] and the blood cells within. Measurements using these imaging modalities are restricted to vessels with a diameter greater than 30 μm. Second, it is difficult to optimize the imaging contrast of retinal capillary and blood flow. The major natural sources of contrast in retinal blood flow images are scattering from the changes of the refraction index and the absorption of (both oxy- and deoxy-) hemoglobin in red blood cells, i.e., the erythrocytes [24]. Image contrast can be severely degraded at longer wavelengths. Imaging methods utilizing advanced molecular techniques to label blood cells or plasma with exogenous contrast agents in animal models cannot be applied to the living human eye [25–28]. For human imaging, we must rely on naturally occurring contrast sources or approved agents, such as indocyanine green (ICG) and sodium fluorescein [29]. These extrinsic dyes enhance visibility of the blood column within the blood vessels but do not provide a way to image the flow or the velocity of erythrocytes. Third, it is challenging to record the spatial positions of the blood cells in the capillaries as these cells are in rapid movement. To avoid motion-blur caused by the relatively long time of photon integration, retinal images should be acquired at high frame rate. However, higher retinal imaging speed has been restricted by equipment limitations such as high frame rate cameras of proper size and resolution, or raster scanning speed. Moreover, imaging with faster frame rates requires greater illumination power so that the detector can collect sufficient photons to render images with good signal to noise ratio; but the imaging light power is restricted by the retinal illumination safety limits [30].

Recent advances in adaptive optics (AO) ophthalmoscopy have overcome some of the aforementioned challenges [31–33]. By correcting for the image blur caused by the optical defects of the human eye (measured as wave aberrations of the imaging light), AO has enabled diffraction limited imaging [34], allowing for resolving the finest capillaries in the living retina. In particular, adaptive optics scanning laser ophthalmoscopy (AOSLO) [35], due to its confocal imaging nature and video rate imaging speed, has been used to study the blood flow in the retinal capillaries of the human eye [36–48]. These studies revealed marked variability in leukocyte velocity and pulsatility between capillaries and between subjects in normal retinae [36–39], identified leukocyte-preferred and plasma-gap-filled capillaries [38], characterized the formation and movement of the erythrocyte aggregates following the leukocytes in the parafoveal capillaries [40–43,47], and measured erythrocyte flow and velocity in retinal arterioles [44, 45] and capillaries [46, 48].

Biomedical Optics EXPRESS

Measuring erythrocyte velocity remains a challenging problem. Erythrocytes constitute 40% to 50% of the blood volume. They are not only the carriers of oxygen and metabolic byproducts but also having their own obvious importance in retinal physiology [49–51]. Accurate measurement of the erythrocyte movement may provide deep insight into normal retinal physiology and pathophysiology. In a pioneering study, Zhong and associates stopped the AOSLO slow scanner during image acquisition to let the fast scanner project a high frequency scanning light line onto a selected blood vessel during the rest of the frame scanning time [44, 45], thereby generating the spatiotemporal traces of the erythrocytes. This clever method allowed for measurement of erythrocyte velocity, but it could work in vessels of 30 - 100 μm in diameter only. Recent development of AOSLO imaging utilizing multiply scattered light has allowed the erythrocytes to be visualized in human retinal capillaries [52]. However, the slow frame rate prevented direct measurement of velocity. Using an AOSLO equipped with two imaging light sources, de Castro and associates recently demonstrated measurements of the velocity of individual erythrocytes traveling in single-file in human retinal capillaries [46]; but it is unclear whether this method can be used to measure blood cell velocity in capillaries containing tightly packed and intertwined erythrocytes [28].

High speed, high resolution retinal imaging that can render instantaneous spatial positions of blood cells in retinal capillaries is attractive for accurate characterization of blood cell movement. Bedggood and Metha demonstrated an AO flood illumination fundus camera operating at 460 frames/second (fps) and measured erythrocyte velocity in retinal capillaries [53, 54]. This pioneering work provided important knowledge regarding erythrocyte motion in retinal capillaries; but it was restricted by the limited capacity of the high speed camera for capturing images over longer periods of time. The image acquisition in this study was limited to 0.13 seconds, which is insufficient for observing erythrocyte motion over longer time. To enhance the contrast of the erythrocytes in the images, they used a light source with wavelength at 593 nm. While this light provided high contrast for imaging erythrocytes within the capillaries, the sensitive (visual) response of the human eye to light at this wavelength makes it difficult to assess the hemodynamic properties of the retina under the natural rheological state without physiological perturbation of the erythrocyte flow by neuronal stimulation. Furthermore, this limitation hindered use of this method for studies involving visually evoked functional changes that occur at longer time scales.

Recently, we have developed a high speed adaptive optics near-confocal ophthalmoscope (AONCO) [55, 56]. This instrument can image the retina at a frame rate up to 800 fps over a field of view of 1.2° × 0.3°. This speed enables direct imaging of the erythrocyte flow in the smallest retinal capillaries. In this study, we use the AONCO to characterize the motion of the erythrocytes within the parafoveal capillaries of the human eye with infrared light that does not visually evoke neuronal activities in the retina.

2. Methods

2.1 The imaging system: the anamorphic AONCO

The instrument is an adaptive optics parallel near-confocal scanning ophthalmoscope [55] with an advanced design of anamorphic imaging, which was reported elsewhere [56]. For the readers' convenience, the working principle and technical characteristics are summarized here.

The AONCO operates with a line scan imaging regime. The imaging light source is a low coherence superluminescent diode (SLD) (Broadlighter S795-HP, Superlum Ltd., Ireland) with a central wavelength of 795 nm and a spectral bandwidth of 15 nm. Light emitted from the SLD is first collimated and then focused by a cylindrical lens to form a line of light on a digital micromirror device (DMD, Texas Instruments, DLP 0.55 XGA Series 450 DMD, Dallas, US). The DMD modulates the light to create a line of point sources. The modulated line light is relayed by the scanning optics (which includes the adaptive optics components) to the eye, generating a 2-D scanning raster on the retina. Light scattered back from the retina

Biomedical Optics EXPRESS

following the ingoing path transmits into the image acquisition module, in which a line camera images the retina through an anamorphic mechanism. Meanwhile, the line image chip of the camera serves as a 1-D confocal gate in the scanning direction. The DMD modulation of the imaging light reduces the light interference on the line image chip (the non-confocal direction), thereby enabling near-confocal imaging in 2 dimensions [55]. The anamorphic imaging mechanism consists of a pair of cross-cylindrical lenses; one (with a focal length of 200 mm) is placed with its cylinder axis parallel to the line camera, while the other (with a focal length of 50 mm) is placed with its axis perpendicular to the line camera [57, 58]. This mechanism provides orthogonally decoupled optical magnifications from the retina to the camera in the direction of the scanning and in the direction of the line camera. The anamorphic ratio of the imaging is 4, which is determined by the power of the two cylindrical lenses. With this configuration, the point spread function (PSF) of the imaging system on the line camera is in a form of an ellipse with a major axis of 70.32 μm (along the line camera) and a minor axis of 17.58 μm (perpendicular to the line camera). The pixel size of the line camera is 10 μm × 10 μm. The camera is set with the vertical dual-line binning mode, i.e., the effective pixel size is 10 μm × 20 μm. Thus, the PSF covers 7 pixels along the line image sensor (with its major axis) and 0.88 pixel perpendicularly (the scanning direction). The line image chip acts as a confocal aperture whose width is 1.14 times of the minor axis of the PSF in the scanning direction. This design ensures sufficient digitization of the optical resolution in the imaging direction (the line camera) [59] and collects the most of light of the PSF.

The AO system consists of a custom Shack-Hartmann wavefront sensor (WS) and a deformable mirror (DM) with 97 actuators (DM, Hi-Speed DM97-15, ALPAO SAS, France). The WS measures the wave aberration by 193 sampling points over a pupil of 6.75 mm (diameter) using a beacon light (λ = 730 nm, SuperK, NKT Photonics AS, Denmark). The DM compensates the wave aberration at a closed-loop frequency of 50 Hz with custom control algorithms [60–63]. In most eyes, the root mean square of the wave aberration after AO compensation can be as low as 0.04 μm, less than 1/14 of the wavelength of the light for wavefront sensing; thus, the imaging can be considered as diffraction limited.

In a normal operational setting of the AONCO, the imaging field of view (FOV) inside the human eye is 1.2° × 1.2°. The image is digitized by 512 × 512 pixels (~0.67 μm per pixel). Under this configuration, the retinal image can be acquired at a frame rate of 200 fps with the signal to noise ratio comparable to that of the images produced by current AOSLO. By reducing the FOV, the images can be acquired at higher frame rates; e.g., with a FOV of 1.2° × 0.6°, the frame rate can be 400 fps, whereas with 1.2° × 0.3°, the frame rate can be 800 fps.

2.2 Human subject study protocol

The study followed the tenets of the Declaration of Helsinki and was approved by the Institutional Review Board for Human Use (IRB) at the University of Alabama at Birmingham. Written informed consent was obtained from the participants after the nature and possible consequences of the study were explained. Seven human subjects with normal healthy retinae were enrolled and the erythrocyte velocity in parafoveal capillaries near the avascular zone were measured.

Retinal image acquisition: The power of the imaging light (λ = 795 nm) was 0.5 mW, which is 0.24 times the ANSI maximum permissible exposures (MPE) under the condition of 1 hour continuous exposure [30, 64]. The power of the wavefront sensing light (λ = 730 nm) was 25 μW, which is less than 1/10 of the ANSI MPE. The composite MPE for multiple light exposure was 0.34 (out of a maximum permissible exposure of 1.0 in this case) [64]. The pupil of the participant was dilated with 1.0% tropicamide and 2.5% phenylephrine hydrochloride. The subject was seated for a period of ~15 minutes prior to imaging in order to establish a stable cardiovascular and respiratory resting state. The subject's head was aligned and stabilized using a head-mount with a chin-rest. An LCD screen (Raspberry Pi 7" LCD Display) presented a flashing green light dot serving as a fixation target to direct the subject's

Biomedical Optics EXPRESS

view direction. The participant looked at the fixation target via a pellicle beam splitter. During imaging, the dot was moved on a calibrated grid.

A typical imaging session includes recording images for generating a map of the parafoveal capillary network and acquiring images for measuring erythrocyte movement. To acquire images for rendering the capillary network, the AONCO was set to its normal operational mode, i.e., with a FOV of 1.2° × 1.2° and a frame rate at 200 Hz. The subject's eye was directed by the fixation target appearing at a grid over an area of 4° × 4° on the retina. At each grid point, the computer recorded 2 – 3 seconds videos with the imaging light focused on the capillaries. To record images for measuring erythrocyte velocity, the AONOCO was set to the high speed mode, with a FOV of 1.2° × 0.3° and a frame rate at 800 Hz. Since the NIR imaging light does not alter the natural rheological state by visually stimulating the retina, videos were recorded over a period of ~10 seconds with the imaging light focused on the capillary bed. The subject was asked to keep their eye stable during the video recording, and they were requested to close eyes and rest for about 60 seconds between video acquisitions.

We have examined the appearance of erythrocytes and leukocytes on the images. To do so, retinal images were acquired with the imaging light focused on the capillaries when imaging the erythrocytes [44, 53, 54] and focused on photoreceptor inner segment plane when imaging the leukocytes [38, 40, 41]. Videos that were approximately 10 seconds long were recorded at 800 fps with the image size of 1.2° × 0.3°.

Electrocardiogram (ECG): A pulse-transducer (TN1012/ST, ADInstruments Inc., Colorado Springs, CO) was attached to the participant's finger to acquire a quasi-ECG signal, which was recorded simultaneously using the data acquisition system (PowerLab 8/35, ADInstruments Inc., Colorado Springs, CO) with the retinal image acquisition. The time series of the ECG was plotted with the blood velocity profile together for analysis.

Ocular biometry and refractive error: Axial length, anterior chamber depth, and corneal curvature were measured before dilation using an ocular biometer (IOL Master 500, Carl Zeiss Meditec, CA). The refractive error was measured using an automated refractor and reported in spherical equivalent power. These parameters were used to calculate the retinal magnification factor from the visual angle [65].

Blood pressure and heart rate measurements: Prior to and after image acquisition, the systolic and diastolic blood pressure and the heartbeats of the participant were measured using a blood pressure monitor (OMRON BP785N, Omron Healthcare, Inc. IL, USA), to ensure there was no dramatic cardiac fluctuation that could affect interpretation of the measurement.

2.3 Generating retinal capillary networks

The capillaries were extracted from the retinal images acquired at 200 fps with a field of view of 1.2° × 1.2°, using motion contrast enhancement [38] through the following steps. First, the background was subtracted from the raw videos. The background image was generated by averaging an image sequence acquired with the imaging light blocked. The images were registered using custom software [66]. Next, a differential video was generated to eliminate the static structure of each frame thereby enhancing regions of high relative motion of the erythrocytes. Then, the vasculature was extracted from the standard deviation of all frames of the differential video. Finally, the retinal capillary network was made by montaging all of the individual images using professional image processing software (Adobe Photoshop cc, Adobe Systems Inc., San Jose, CA).

2.4 Creating 2-D spatiotemporal traces of the blood cells

The spatiotemporal traces of blood cells traveling through the retinal capillaries were derived from the videos following published methods using custom software [38, 39, 67]. Briefly, for the blood flow in a segment of capillary of interest, the vessel centerline was first drawn on

Biomedical Optics EXPRESS

the image of the capillary network map. Then, the values of the pixels on the centerline were read out from sequential frames and plotted against the frame number, forming a 2-D image. This image revealed a series of sloped hyper-reflective or hypo-reflective lines starting at one end of the plot and finishing at the other end. These sloped lines represented the spatiotemporal traces of the blood cells that moved through the vessel. The intensity variation of the spatiotemporal image caused by the non-uniform illumination of the imaging light (whose intensity distribution was a Gaussian function along the light line) was corrected using methods reported by Duncan and colleagues [68].

2.5 Characterizing the movements of erythrocytes

Measuring erythrocyte velocity using the Radon transform: the slopes of spatiotemporal traces of the erythrocytes represent the blood velocity. We have developed custom software to measure the trace slopes based on the Radon transform, which provides a robust method for measuring the angles of the traces. The Radon transform of a 2-D image $R(\rho,\theta)$ is a projection of the image in a series of angles ((ρ, θ) are coordinates in the Radon space). The projection is the summation of the pixel values of every lines on a given angle θ, and ρ is the length of the projection. The local maximum of the Radon transform indicates the projection angle that best matches the spatiotemporal traces of the erythrocytes [54, 68]. An illustration of the method using the Radon transform to measure the erythrocyte flow velocity is presented in Appendix 1 (Fig. 12).

Optimizing the sampling window: to measure the instantaneous velocity of the erythrocytes accurately, we optimized the sampling window size in a set of spatiotemporal plots using the following merit function M,

$$M = \frac{1}{N}\sum_{n=1}^{N}\left\{\max_{1\ll i\ll q}\left\{\sqrt{\frac{1}{p}\sum\nolimits_{j=1}^{p}R(\rho_j,\theta_i)^2}\right\}\Big/\sqrt{\frac{1}{pq}\sum\nolimits_{i=1}^{q}\sum\nolimits_{i=1}^{q}R(\rho_j,\theta_i)^2}\right\}_n$$

where n denotes the sampling point on the time axis of the spatiotemporal plot at which the velocity is measured. N is the total number of sampling points. p and q are the dimensions of the Radon transform. The merit function is the average of the normalized maximum Radon transform values at all measurement points of the spatiotemporal plot [54]. In other words, an optimal sampling window will ensure that the Radon transform achieves an overall maximum value over all points measured. The merit function is explained in detail in Appendix 2.

Assessing the impact of imaging speed on velocity measurement: we recorded the retinal images from the human eye at 800 fps. By dropping intermediate frames, we generated videos with equivalent frame rates of 400 fps and 200 fps from the same imaging period, extracted spatiotemporal plots from the videos of different frame rates, and then measured the velocities under different frame rates. To assess the impact of the frame rate on velocity measurement, we calculated the correlation coefficients of the velocity waveforms measured in images of 200 fps and 400 fps to those obtained in images of 800 fps.

Measuring the dynamic characteristics of erythrocyte motion: In addition to conventional metrics of the velocity, such as the maximum (systolic) velocity (V_{max}), minimum (diastolic) velocity (V_{min}), mean velocity (V_m), pulsatility index [36–38], we introduced 2 new metrics, namely, erythrocyte acceleration time (T_r) [69] and the erythocyte velocity rising rate (R_r) [69]. T_r measures the time of the erythrocytes being accelerated from the diastolic state to the systolic state. R_r estimates the distance that the erythrocytes travel over the time being accelerated from the diastolic state to the systolic state. All parameters were measured form the averaged velocity waveform of multiple cardiac cycles. The number of erythrocytes was counted in each cardiac cycle from the spatiotemporal plots of the capillaries containing single file cells and the average number was reported.

Measuring capillary lumen diameter: Following published methods [70], the blood vessel's intensity profile was fitted with a Gaussian function with a standard deviation of σ.

Biomedical Optics EXPRESS

We took the image point at which the light intensity of the lumen exhibiting the maximum change as the lumen boundary (at one side), which corresponds to a point where the Gaussian curve (function) has the maximum curvature. We used the full width at the maximum curvature point ($2 \times 1.78\sigma$) of the Gaussian curve as the lumen diameter of the blood vessel.

3. Results

3.1 AONCO enabled direct imaging of erythrocyte flow in retinal capillaries

Anamorphic imaging significantly improved the light collection efficiency and allowed for direct imaging of the blood flow in the retinal capillaries. The supplemental videos show representative erythrocyte flow images acquired at 200 fps, 400 fps, and 800 fps, with the image FOV set as 1.2° × 1.2° (512 × 512 pixels), 1.2° × 0.6° (512 × 256 pixels), and 1.2° × 0.3° (512 × 128 pixels), respectively. Figure 1 shows the macular capillary network.

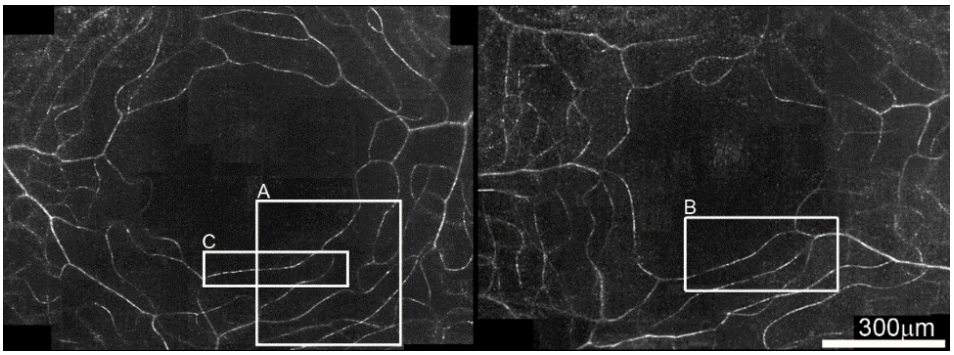

Fig. 1. The parafoveal capillary network generated by the motion contrast enhancement method. Images were taken from 2 eyes of 2 human subjects with normal macular health. The scale bar applies to both panels. The videos in the boxes A (see Visualization 1), B (see Visualization 2), and C (see Visualization 3) were acquired at 200 fps, 400 fps, and 800 fps, respectively, but all are displayed at 30 fps.

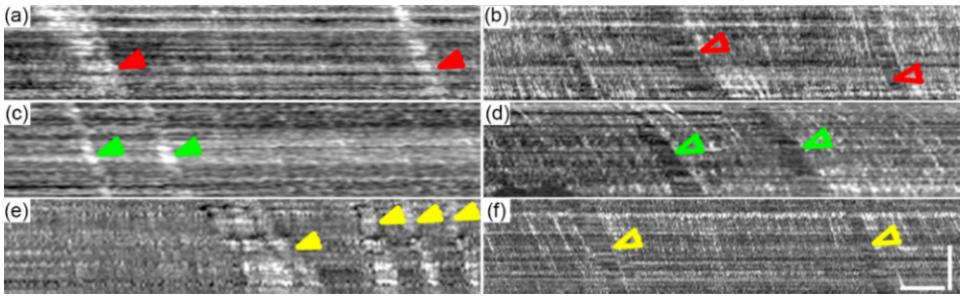

Fig. 2. Spatiotemporal traces of the blood cells when the imaging light was focused on different planes. The plots in each row were generated from the videos taken in the same capillary. Left column panels were blood cells traces when the light was focused on the photoreceptor inner segment plane. Due to low absorption and scattering, the leukocyte traces appear as hyper-reflective bands indicated by solid color arrowheads. Right column panels were made from videos with light focused on the capillaries directly. Due to higher scattering rate, the erythrocyte formed hyper-reflective lines separated by narrow dark gaps generated by plasma. When leukocytes pass through the capillary, because of their low absorption and low scattering and confocal rejection of scattering out-of-focus, they appear as broad hypo-reflective bands (pointed by the empty arrowheads) followed by densely packed hyper-reflective lines, which are accumulated erythrocytes. Arrowheads with same color indicate leukocytes in the same capillary. Because the videos were not taken simultaneously, the leukocytes in the same capillary are not the same cells. All images were generated from videos acquired at 800 fps. The spatial (vertical) scale bar is 25 μm and the temporal (horizontal) scale bar is 100 ms.

Biomedical Optics EXPRESS

3.2 High speed imaging revealed characteristic spatiotemporal traces of the erythrocytes and the leukocytes in retinal capillaries

As shown in Fig. 2, when the imaging light was focused on the photoreceptor inner segment plane, the spatiotemporal traces of the leukocytes appear as hyper-reflective bands (solid arrowheads, panels in left column), whereas the traces of the erythrocytes as well as the plasma are not discernable. This phenomenon has been well-described by Uji et al and Arichika et al [40, 41]. Due to low absorption and scattering of the imaging light, the leukocytes allowed more imaging light to pass through them and reached the photoreceptors. Meanwhile, in the reversed direction, more back-scattered light from the photoreceptors could transmit through the leukocytes and reached the camera, thereby forming a hyper-reflective spot on the blood flow image. Alternatively, when the imaging light was focused on the capillaries, the erythrocytes caused much stronger scattering (10^2 – 10^3 times) than leukocytes and plasma [24, 71]. Thus, the erythrocytes appeared as small bright particles moving in the capillary. These bright particles were separated by dark gaps, which were plasma. When leukocytes passed through the capillary, because of low absorption and low scattering as well as confocal gate rejection of light out-of-focus, they appeared as large dark spots followed by bright erythrocyte (aggregation) bands. Under this condition, on the spatiotemporal plot, the traces of the leukocytes appear as hypo-reflective bands followed by hyper-reflective bands formed by the accumulation of following erythrocytes, as illustrated in the right column panels of Fig. 2.

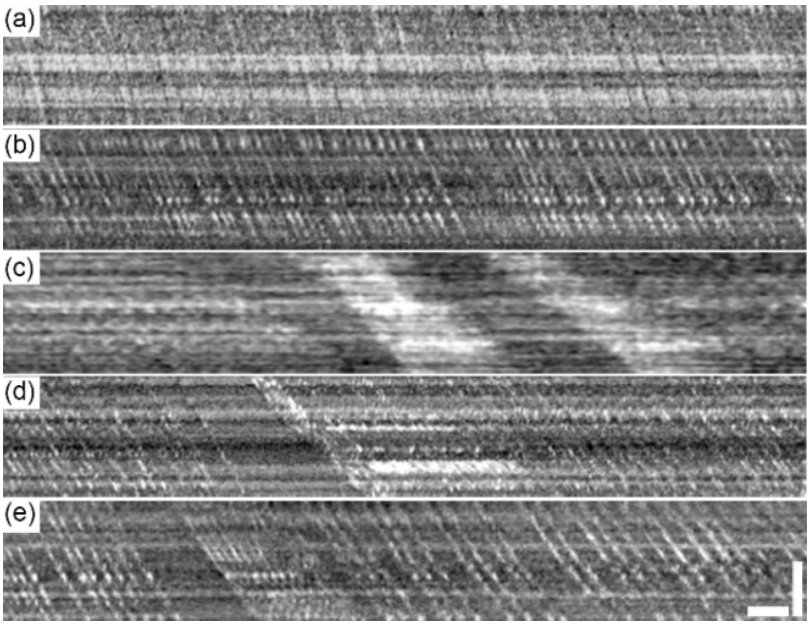

Fig. 3. Characteristic spatiotemporal traces of the erythrocytes in retinal capillaries obtained from the AONCO imaging. (a) Type 1, the blood flow in the capillary contained densely packed erythrocytes flowing in non-single files and no leukocytes. (b) Type 2, the blood flow contained erythrocytes flowing in single files and no leukocytes. (c) Type 3a, the blood flow contained both leukocytes (hypo-reflective bands) and non-single file erythrocyte aggregation (hyper-reflective bands). (d) Type 3b, the blood flow contained both leukocytes (hypo-reflective bands) and light erythrocyte aggregation (hyper-reflective bands). (e) Type 4, the blood flow contained leukocytes accompanied by non-aggregated upstream erythrocytes. All spatiotemporal plots were extracted from retinal images acquired at 800 fps, with the imaging light focused on the capillary bed. The temporal (horizontal) scale bar indicates 25 ms and the spatial (vertical) scale is 25 μm.

Biomedical Optics EXPRESS

Figure 3 shows characteristic spatiotemporal traces of erythrocytes and leukocytes generated from images acquired with the imaging light focused on the capillaries. In general, the erythrocyte traces are hyper-reflective and the leukocyte traces are hypo-reflective. Dense hyper-reflective bands represent erythrocyte aggregations. Based upon the erythrocyte and leukocyte arrangement patterns in the retinal capillary, we classified the blood flow into 4 categories, as shown in Fig. 3. The type 1 (Fig. 3(a)) and type 2 (Fig. 3(b)) flow patterns may correspond respectively to the 'zigzag configuration' and the 'parachute configuration' of the erythrocyte arrangement that have been noted by Guevara-Torres and associates [28]. Plasma possesses similar absorption and scattering rates to those of leukocytes. Thus, they appear as dark spaces between erythrocytes [38]. In total, out of 92 capillaries (10 – 20 capillaries/subject) imaged in 7 subjects (whose were 24 – 53 years old), we identified that 31 capillaries as type 1, 41 as type 2, 11 as type 3, and 9 as type 4. In capillaries containing erythrocytes flow in single file (types 2 and 4, Figs. 3(b) and 3(e)), the cell flux can be unambiguously counted (Fig. 4).

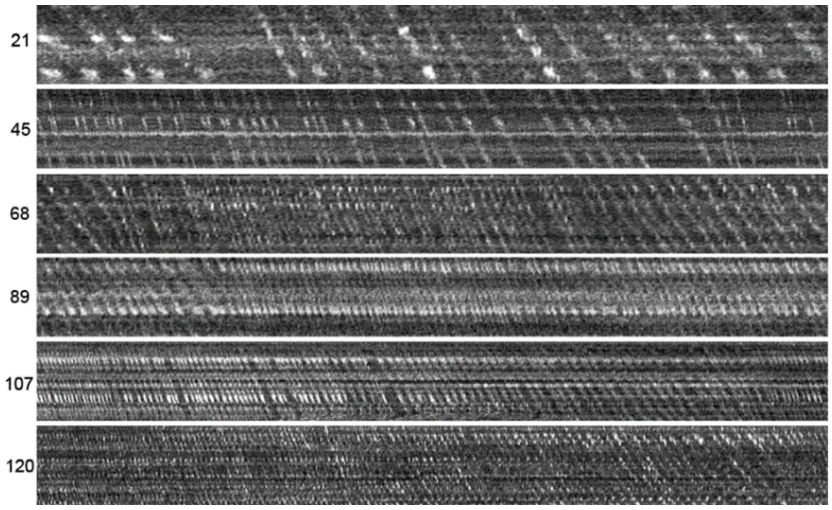

Fig. 4. Spatiotemporal traces of the erythrocyte flow in capillaries with different cell flux. Each plot represents the erythrocyte flow in one cardiac cycle (horizontal). All panels have been adjusted to be of the same size for display purpose. The numbers on the left are the erythrocytes counted within one cardiac cycle. All spatiotemporal plots were extracted from retinal images acquired at 800 fps, with the imaging light focused on the capillary bed.

3.3 Optimal sampling window size for measuring the erythrocyte velocity

We calculated the merit function at the sampling points on the time axis of the spatiotemporal plots derived from videos acquired at 800 fps over 15.32 seconds. The sampling frequency of the velocity measurement was set to 100 Hz, which was equal to the sampling frequency of the ECG signal recording. The sampling window size was varied from 25 ms to 150 ms with an increment of 12.5 ms. For each spatiotemporal plot, we assessed the merit function at 1532 time points, using 11 sampling windows of different sizes (total 16852 testing points). Figure 5 shows the merit function averaged from 3 videos. The sampling window with a size of 75 ms yielded the maximum value, which was used to measure the velocity through this study.

Biomedical Optics EXPRESS

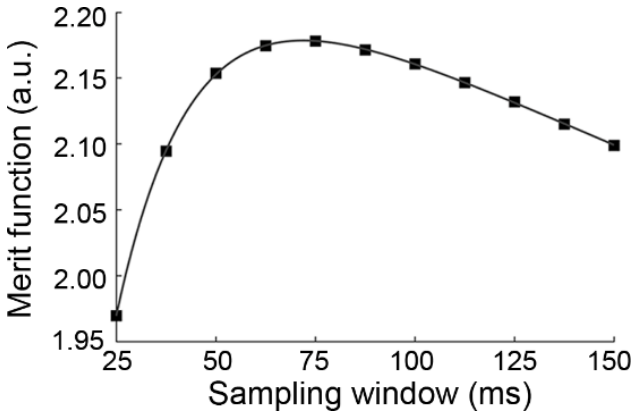

Fig. 5. The merit function under different sampling windows.

3.4 Impact of imaging speed on blood velocity measurement

Figures 6 and 7 show the comparison of the erythrocyte velocity measured in the same capillary with retinal images of different frame rates. When the maximum velocity is less than 3 mm/s, the velocity waveforms measured from images of 400 and 800 fps agree with each other well (Fig. 6). The examination of the erythrocyte velocity in 7 capillaries of 6 subjects has yielded a correlation (between velocity waveforms of 400 and 800 fps) coefficient that was greater than 92.7%. However, with the images of 200 fps, the correlation (between velocity waveforms of 200 and 800 fps) coefficient was up to 54.5% only. The velocity (waveform) measured in images of 200 fps often exhibited significant aliasing compared to those measured in images of 400 fps or 800 fps. As shown in Fig. 6(b), the spatiotemporal traces generated from the images of 200 fps (the red box) manifest clear aliasing of slope.

Biomedical Optics EXPRESS

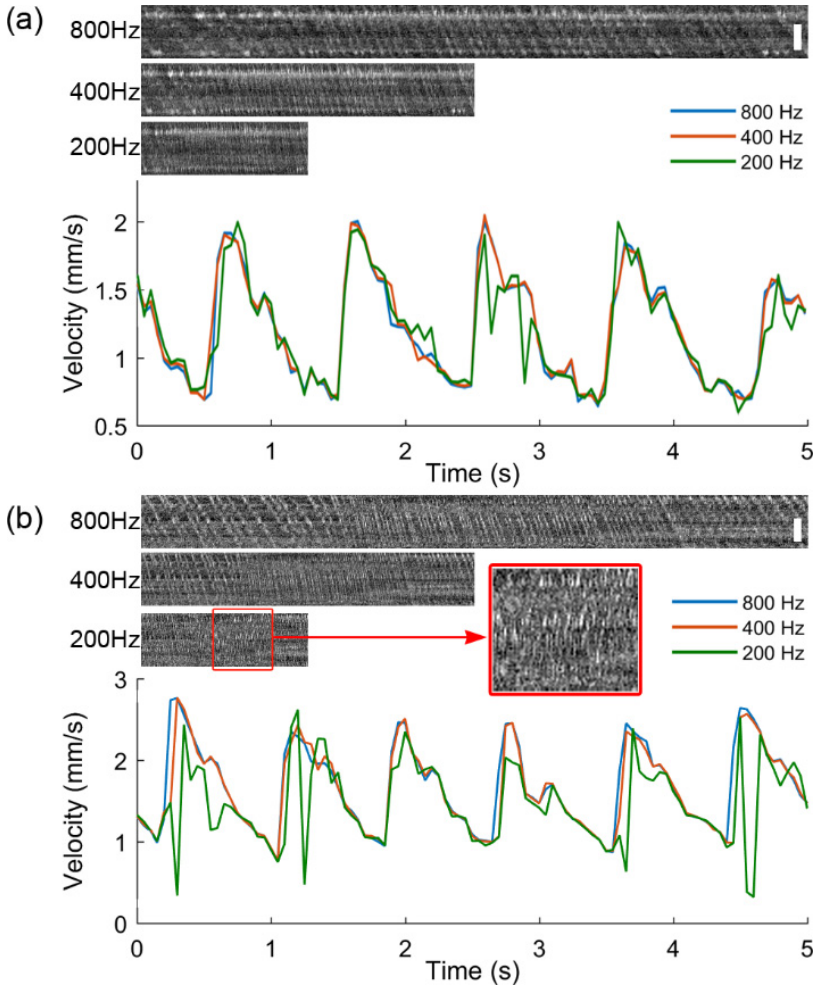

Fig. 6. Erythrocyte velocity measured by retinal imaging at frame rates of 800 fps, 400 fps, and 200 fps. (a) Erythrocyte flow in a capillary with the maximum velocity < 2mm/s. (b) Erythrocyte flow in another capillary with the maximum velocity between 2 and 3mm/s. The retinal images were acquired at the frame rate of 800 fps with the imaging light focused on the capillary bed. Retinal images of 400 fps and 200 fps were generated by dropping off the intermediate frames from the images of 800 fps. The spatiotemporal plots were extracted from corresponding videos. The time span of the spatiotemporal plots is 1 cardiac cycle. The spatial scale bar is 25 µm.

In our study, the maximum velocity of capillary blood flow was higher than previous publications [46, 53]. In 6 (of 92) capillaries, the maximum velocity was found to be greater than 4 mm/s (Fig. 7). In these cases, the velocity could not be measured in images of 200 fps. While the velocity could be measured in images of 400 fps, the waveforms have exhibited aliasing when compared to images acquired at 800 fps. To measure the velocity correctly, high frequency aliasing must be removed by applying proper time filters [72]. To test the measurement capacity, we measured the blood velocity in a 3rd order arterial at 800 fps (Fig. 8), where the maximum velocity reached 10 mm/s. In this study, the diameters of capillaries were 5.8 ± 0.7 µm (which are smaller than the diameter of the 3rd order arterial). Thus, our measurement of the maximum velocity in these capillaries was not clipped by the imaging speed. In general, we believe that imaging at 400 fps may provide accurate measurement of the erythrocyte velocity in the retinal capillaries (the 4th and 5th order vessels).

Biomedical Optics EXPRESS

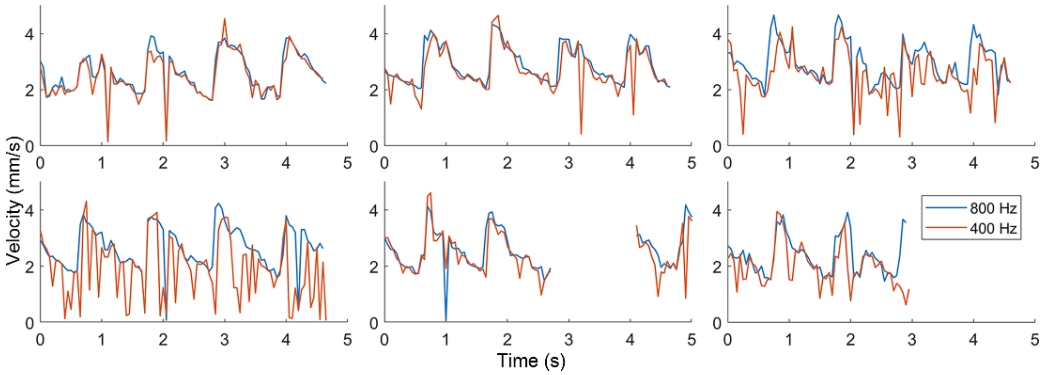

Fig. 7. A comparison of the erythrocyte velocity measured with imaging at frame rates of 800 fps and 400 fps. In these 6 capillaries, erythrocyte maximum velocity was found to be > 4 mm/s. The retinal images were acquired at the frame rate of 800 fps. Retinal images of 400 fps were generated by dropping off the intermediate frames of the images acquired at 800 fps. The gap in the bottom middle panel was caused by eye blinking.

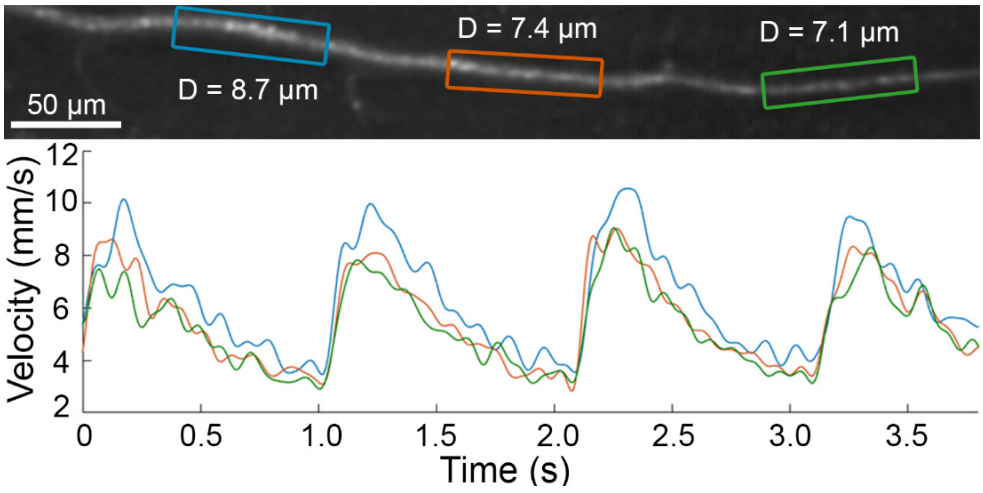

Fig. 8. Measuring the blood velocity in an arterial. The velocity was measured in 3 segments (colored boxes) of the vessel using images acquired at 800 fps with the imaging light focused on the vessel. D is the dimeter of the blood vessel. Instantaneous velocity up to 10 mm/s can be measured.

3.5 High speed imaging disclosed fine movement of erythrocytes and leukocytes

Many leukocytes are larger than erythrocytes [73] and must be compressed more in order to pass through the capillaries. Thus, they may potentially slow down the following erythrocytes and plasma. When blood cells meet at a confluence point from 2 capillaries, interference between two streams may temporarily block the blood flow. Sometimes, the erythrocytes may be arrested within capillaries. Figure 9 illustrates these processes.

Biomedical Optics EXPRESS

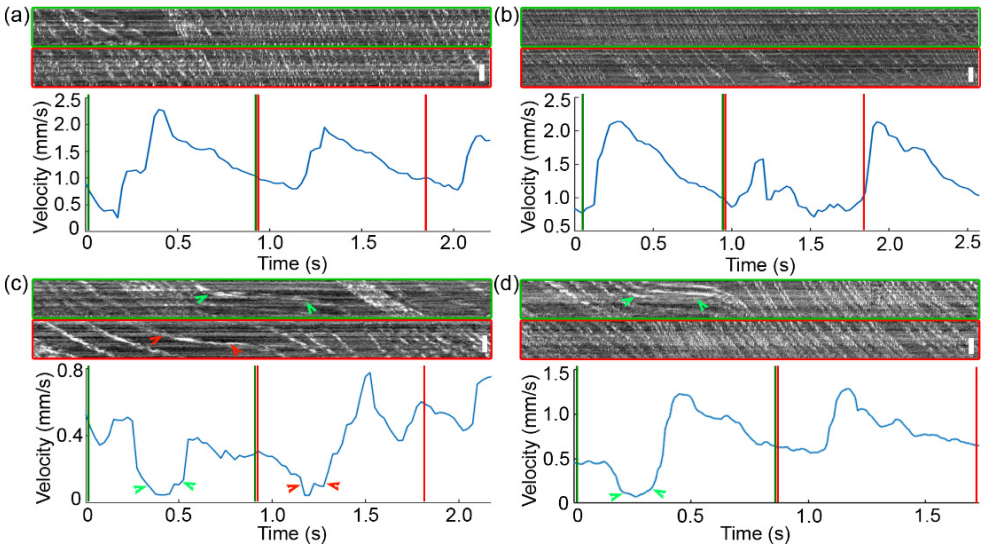

Fig. 9. High speed imaging revealed fine movement of the erythrocytes. (a) The erythrocytes movement was slowed down by a leukocyte appeared at the beginning of the first cycle (the green box). (b) The erythrocytes movement was distorted by leukocytes (hypo-reflective bands in the red box). (c) Temporary blood cell traffic jam at the vicinity of a confluence point (Visualization 4, acquired at 400 fps with a field of view of 1.2° × 0.6°, displayed at 30 fps), causing almost stoppage of the blood flow and nearly flat spatiotemporal traces (green and red arrowheads). (d) Temporal arresting of the erythrocytes (Visualization 5, acquired at 800 fps, displayed at 30 fps). All spatiotemporal plots were extracted from retinal images acquired with the imaging light focused on the capillary bed. The velocity waveforms in the regions indicated by the color lines were measured from the boxes of corresponding color. Scale bar is 25 µm.

In Fig. 9(a), due to the presence of a leukocyte at the beginning of the 1st cycle (green box), the minimum velocity of the erythrocytes was slowed down to 0.39 mm/s. After the passage of the leukocyte, the minimum velocity became 0.78 mm/s in the 2nd and 3rd cycles. In Fig. 9(b), overall movement of the erythrocytes in the 2nd cycle (red box) was distinctively slowed down in comparison to that in adjacent cycles, due to the presence of possibly 2 leukocytes. In Fig. 9(c), blood cell interactions at the confluence point transiently caused near-cessation of the blood flow. The corresponding spatiotemporal traces of the erythrocytes became near-horizontally oriented (indicated by colored arrowheads) during this time. Figure 9(d) demonstrates a temporary arresting of the erythrocytes lasting for ~0.25 second (marked by green arrowheads). This case was only observed once in the 92 capillaries of the 7 subjects.

3.6 High speed imaging revealed cardiac-dependent pulsatile erythrocyte movement

High speed NIR imaging allowed for recording the erythrocyte flow over time without disturbing normal physiological state of the retina. The erythrocyte velocity measured from the continuously recorded retinal images revealed a distinctively pulsatile waveform. This result confirmed the observation made by de Castro and associates [46]. Furthermore, our measurement proved that the velocity fluctuation was cardiac dependent. As can be seen in Fig. 10, although the velocity waveforms of the erythrocytes in 3 capillaries have different maximum, minimum, and mean values, they were synchronized with the ECG, which reflected the electrical activity of the heartbeat.

Biomedical Optics EXPRESS

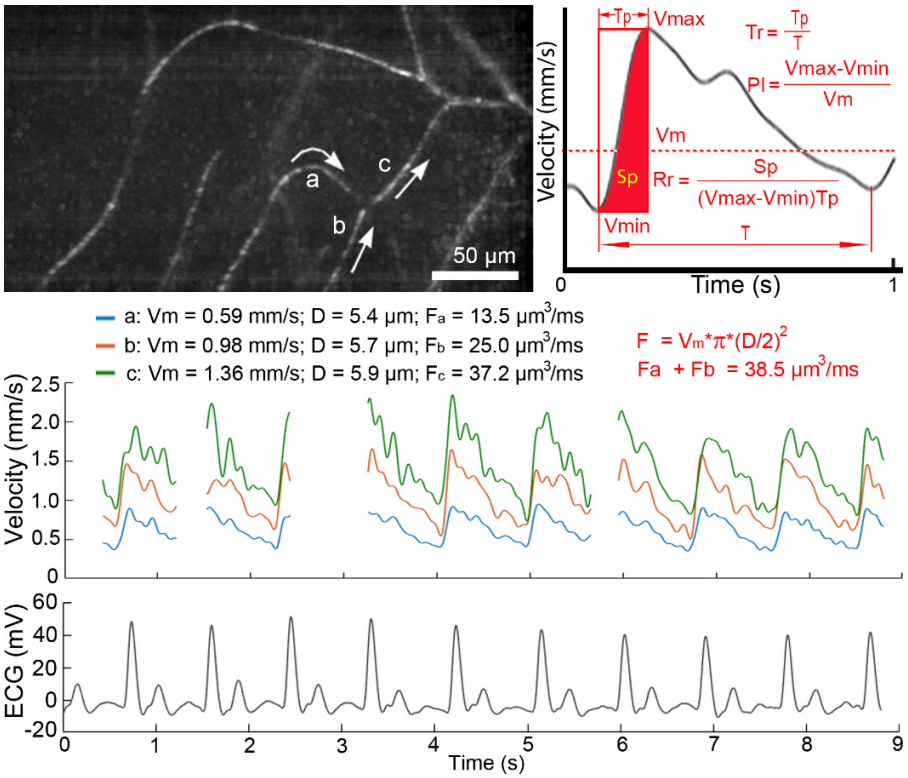

Fig. 10. Cardiac-dependent velocity fluctuation of the erythrocyte in retinal capillaries. Top left panel shows 3 capillaries within which the erythrocyte velocity was measured. White arrows indicate the flow directions. Middle panel shows the velocity waveforms measured in the 3 capillaries. Gaps in the waveforms were caused by eye blinks during imaging. Bottom panel is the ECG that was recorded simultaneously with the retinal images. Top right panel illustrates the velocity waveform averaged from multiple cardiac cycles. V_{max}: the maximum velocity. V_{min}: the minimum velocity. V_m: the mean velocity. PI: Pulsatility index of the blood flow. T_p: the time span over which the erythrocyte velocity is accelerated from V_{min} to V_{max}. T: cardiac period. T_r: acceleration time index of the erythrocytes, which is a measure of the interaction between the erythrocytes with the blood vessels. S_p: the distance that the erythrocytes have flowed in the blood vessel during the period of being accelerated within a cardiac cycle. R_r: the raising rate of the erythrocyte velocity, which is a normalized measure of the distance that the erythrocytes travel within a cardiac cycle. F_a, F_b, F_c: flow rates in vessels a, b, and c, respectively. D: the diameter of the capillary. The blood flow was calculated using the formula $F = v_m \pi D^2/4$, assuming that the capillaries were cylindrically symmetric, with a round cross-section shape. The retinal images were acquired with the imaging light focused on the capillaries.

3.7 High speed imaging confirmed conservation of blood flow in the confluence and bifurcation points

To test the accuracy of the measurement of blood flow, we examined the flow conservation relationship in retinal capillaries near the confluence and bifurcation points. In Fig. 10, the blood flows in 2 capillaries (a and b) converged into a slightly larger one (c). The diameters of the 3 vessels are smaller than the average size of erythrocytes. The measured difference in conservation of flow was 3.4% in the convergent branch. In Fig. 11, the blood flow in a larger capillary (with a diameter close to the typical size of erythrocytes) was split into 2 smaller ones. The conservation relationship error was 4.1%. These results are similar to those reported by Guevara-Torres and associates [28]. The errors may be caused by the following factors. First, the estimation was made under the assumptions that the capillaries were

Biomedical Optics EXPRESS

cylindrically symmetric and with a round cross-section shape. Thus, uncertainties in true lumen diameter may affect the accuracy of the assessment. Second, some capillaries may not be entirely planar but change in depth.

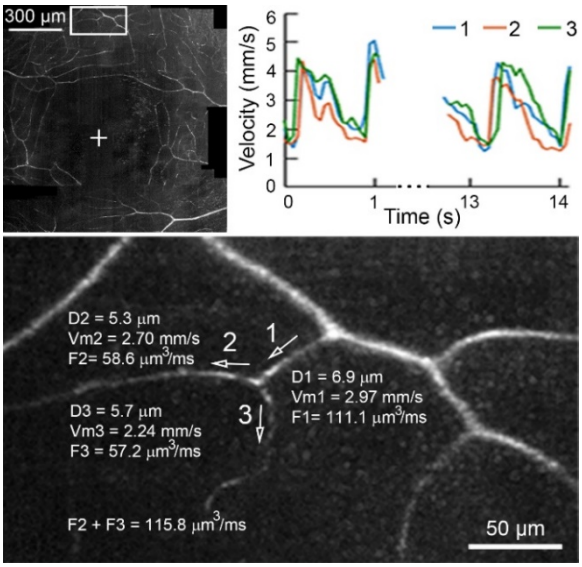

Fig. 11. Conservation of blood flow in the bifurcation. White arrows indicate the flow directions in 3 capillaries. F1 – F3: flow rates in capillaries 1, 2, and 3, respectively. D1 – D3: diameters of the capillaries. V_{m1} – V_{m3}: mean velocities of the erythrocytes in the corresponding capillaries. The blood flow was calculated using the formula $F = v_m \pi D^2/4$, assuming that the capillaries were cylindrically symmetrical and with a round cross-section shape. The retinal images were acquired with the imaging light focused on the capillaries.

3.8 Measurement of the dynamic characteristics of the erythrocyte motion

Seven subjects with normal ocular health were enrolled in the measurement (Table 1). Ninety-two (n = 92) capillaries in the 7 subjects were assessed. Table 2 shows the hemodynamic characteristics measured in one capillary over 5 consecutive cardiac cycles.

Table 1. Subject characteristics

	Age (years)	Axial length (mm)	Mean arterial blood pressure (mm Hg)	Spherical equivalent (Diopters)	Heart rate (bpm)
Mean ± SD	36.6 ± 14.0	24.32 ± 0.83	81.4 ± 7.8	–0.71 ± 0.83	64.9 ± 9.0
Range	24.0 – 53.0	22.74 – 25.55	70.4 – 90.2	–1.75 – –0.75	48.0 – 73.0

SD: standard deviation.
bpm: beats per minute.

Table 2. Dynamic characteristics of the erythrocyte flow in one capillary

Cardiac cycle	V_{max} (mm/s)	V_{min} (mm/s)	V_m (mm/s)	Pulsatility index (PI)	Acceleration time index (T_r)	Rising rate (R_r)	Erythrocytes per cardiac cycle
1	2.23	0.99	1.51	0.80	0.17	0.50	73
2	2.11	0.93	1.50	0.76	0.19	0.54	76
3	2.30	1.05	1.58	0.77	0.19	0.52	74
4	2.41	0.99	1.57	0.87	0.19	0.52	77
5	2.30	1.07	1.60	0.75	0.17	0.51	78
Mean	2.27	1.00	1.55	0.79	0.18	0.52	76
SD	0.10	0.05	0.04	0.05	0.01	0.01	2
COV	0.04	0.05	0.02	0.06	0.06	0.02	0.03

SD: standard deviation.
COV: coefficient of variation.

Biomedical Optics EXPRESS

The averaged hemodynamic characteristics in 7 eyes of 7 subjects are presented in Table 3. Table 4 presents a comparison of the blood velocity and the pulsatility index measured in this study with those reported in previous studies. In particular, to compare our measurement with the pioneering work of de Castro and associates [46] as well as Bedggood and Metha [53], we also measured the velocity and pulsatility index in 41 capillaries that contained well-separated single file erythrocytes.

Table 3. Dynamic characteristics of the blood flow in 7 subjects

Subject	V_{max} (mm/s)	V_{min} (mm/s)	V_m (mm/s)	Pulsatility index (PI)	Acceleration time index (T_r)	Rising rate (R_r)	Erythrocytes per cycle
1	2.44 ± 1.20	1.17 ± 0.58	1.75 ± 0.86	0.73 ± 0.08	0.13 ± 0.03	0.50 ± 0.08	57.5 ± 26.3
2	1.85 ± 0.46	0.82 ± 0.20	1.28 ± 0.30	0.80 ± 0.06	0.17 ± 0.04	0.45 ± 0.08	83.6 ± 22.2
3	2.41 ± 0.79	1.02 ± 0.38	1.60 ± 0.56	0.88 ± 0.11	0.15 ± 0.03	0.49 ± 0.07	66.3 ± 15.1
4	2.14 ± 0.64	1.09 ± 0.34	1.51 ± 0.44	0.70 ± 0.08	0.20 ± 0.06	0.54 ± 0.09	60.8 ± 20.2
5	2.55 ± 1.04	0.92 ± 0.33	1.65 ± 0.65	0.95 ± 0.19	0.15 ± 0.04	0.47 ± 0.05	38.5 ± 16.2
6	2.54 ± 0.65	0.88 ± 0.34	1.52 ± 0.42	1.11 ± 0.23	0.21 ± 0.04	0.60 ± 0.06	75.5 ± 19.4
7	1.77 ± 0.53	0.69 ± 0.22	1.10 ± 0.33	0.99 ± 0.20	0.20 ± 0.04	0.60 ± 0.05	76.6 ± 22.2
Mean	2.24	0.94	1.49	0.88	0.17	0.52	65.5
SD	0.30	0.15	0.21	0.14	0.03	0.06	14.0
COV	0.13	0.16	0.14	0.15	0.16	0.11	0.21

SD: standard deviation.
COV: Coefficient of variation.

Table 4. Dynamic characteristics of the blood flow: a comparison with published data [Mean (Range)]

	V_{max} (mm/s)	V_{min} (mm/s)	V_m (mm/s)	Pulsatility index
All vessels [a]	2.24 (0.80 – 4.24)	0.94 (0.32 – 1.96)	1.49 (0.51 – 2.83)	0.88 (0.57 – 1.57)
Erythrocytes only [b]	1.88 (0.80 – 3.35)	0.76 (0.37 – 1.20)	1.22 (0.58 – 1.98)	0.91 (0.63 – 1.57)
de Castro et al [46]	1.88 (0.71 – 3.98)	0.82 (0.26 – 1.99)	1.14 (0.30 – 2.26)	0.79 (0.48 – 1.28)
Bedggood and Metha [53]	(0.60 – 3.30)[c]	(0.30 – 1.50)[c]	1.33 ± 0.28	
Tam et al [38]			(1.30 – 1.80)	(0.54 – 0.61)
Arichika et al [41]			1.49 (0.79 – 2.19)	
Arichika et al [42]			1.02 (0.13 – 2.21)[d]	
Uji et al [40]			1.34 (0.73 – 2.36)	
Martin and Roorda [36]	(?– 3.28)	(0.34 – ?)	1.30 (0.93 – 1.94)	0.45 (0.31 – 0.65)
Martin and Roorda [37]	(1.08 – 2.10)	(0.77 – 1.75)	1.37 (0.94 – 1.95)	

a. The mean and range values were measured in 92 studies vessels.
b. The mean and range values were measured in 41 vessels that contained well-separated single file erythrocyte flow (type 2 spatiotemporal plot, as shown in Fig. 3(b)).
c. The data were read from Fig. 6 of Ref. [53].
d. The data were calculated from all the subjects in Table 1 of Ref. [42]. The upper and lower bounds of the range were estimated using Mean ± 2 SD.

4. Discussion

We present a noninvasive method for characterizing erythrocyte motion in retinal capillaries in the living human eye. AO compensation for ocular wave aberration ensured that the erythrocyte flow was imaged in the smallest retinal capillaries. High speed near-confocal imaging facilitated generation of the spatiotemporal traces of the erythrocytes, allowed for direct and accurate measurement of the erythrocyte velocity, and revealed a distinctively cardiac-dependent pulsatile velocity waveform that was seen in large blood vessels [44]. Imaging with high temporal frequency provided new parameters for precise characterization of erythrocyte movement in the retinal capillaries.

4.1 High speed near-confocal imaging vs. high speed flood illumination imaging

Our study expanded the pioneering work of Bedggood and Metha [53, 54] in several ways. First, our imaging system was working with a near-confocal mechanism. A major advantage was that the confocal gate improved imaging contrast in comparison to the flood illumination imaging. When the light was focused on the retinal capillary, light scattered by the

Biomedical Optics EXPRESS

photoreceptors was largely blocked by the confocal gate, erythrocytes caused stronger scattering than leukocytes, platelet, and plasma thus they were imaged with positive contrast in the capillary. We were able to extract the spatiotemporal traces of the blood cells directly from the raw images without extra work for contrast enhancement. By properly adjusting the light focusing plane using the deformable mirror, we could image virtually any capillary in the macula. Second, we used a NIR light source to image the retina thereby avoiding the adverse effect of visible light, such as visually evoked response [53] and phototoxicity concerns [74]. This allowed for recording of erythrocyte movement in the living human eye over time without exogenous contrast agents or elicitation of neuronal activities. Third, we used of a low coherence SLD as the imaging light source and employed a DMD imaging light modulation mechanism thereby effectively reducing light interference in the image. This enhancement ensured imaging of individual erythrocytes that flowed in single file (the 'parachute' arrangement [28]) in retinal capillaries.

High speed image acquisition in this study was achieved through line scan imaging. A drawback of this imaging mechanism is low efficiency of imaging light collection while maintaining adequate digitization of the optical resolution. In our earlier development of AO line scan imaging, the system had to be configured with a hyperconfocal setting so that the optical resolution can be sufficiently digitized. The line image sensor (width) that served as the confocal gate was of 0.28 – 0.45 times of the PSF of the imaging system [55, 75]. The hyperconfocal setting resulted in significant light loss, hindering high speed imaging due to insufficient imaging SNR. In the present instrument, the anamorphic imaging 'compressed' the light of all the PSF into the image sensor thereby significantly increasing the light collection, which ensured retinal images acquired at 200 FPS with the SNR comparable to that of current AOSLO imaging. By reducing the region of interest to 1.2° × 0.3° (similar to the image size reported by Bedggood and Metha [53]) we could acquire retinal images at 800 FPS. With this ability, we were able to estimate the impact of the imaging speed on the measurement of the erythrocyte velocity and calibrate the measurement accuracy by examination of the conservation of blood flow in the convergence and bifurcation capillary branches.

4.2 High speed near-confocal imaging vs. dual-wavelength AOSLO

Our work extended the important findings made by de Castro and associates [46]. We observed continuous and cardiac-dependent pulsatile velocity waveforms, which confirmed the observations of de Castro and colleagues [46]. Furthermore, in capillaries containing well-separated single file erythrocytes, we were able to quantify the cell flux. High speed near-confocal imaging developed in this study allowed us to measure the velocity of erythrocytes in virtually all capillaries, not limited to those contain single file erythrocytes. However, the erythrocytes imaged by our instrument are not comparable, in terms of clarity and specificity, to those imaged by the AOSLO using multiply scattered light, as presented by de Castro and associates [46].

4.3 Comparison with other methods for measuring blood velocity and pulsatility

Compared with other approaches that measure the blood velocity in retinal capillaries with AO imaging of leukocytes [36–38, 40, 47], a clear feature of this study is that we used the erythrocytes as the proxy. Our method filled the technical niche that measuring the erythrocyte movement in retinal capillaries with diameter < 10 μm. OCT angiography has provided a transformative tool to map vascular perfusion at the structural and qualitative functional level [76–79], but it has not yet provided quantitative assessment of capillary flow in the human retina due to limited spatial resolution and imaging speed. Overall, OCT angiography provides important information of the 3-D architecture of the capillary bed. The method presented in this paper offers complementary or advanced assessment of the physical status of the capillaries associated with or before the structural change. In the future, the high

Biomedical Optics EXPRESS

sensitivity of the AO imaging for visualizing the vasculature and assessing hemodynamics through the capillaries may be useful for validating or better interpretation of findings obtained through OCT angiography.

4.4 Observing important findings made in animal models in the living human eye

The method presented in this study allowed the important knowledge learned in animal models [25–28] to be examined in the living human retina. Recently, Guevara-Torres and associates reported a comprehensive measurement of the blood cell flux, morphology, class, velocity, and rheology in the living mouse eye [28]. With the spatiotemporal plots generated from high speed imaging, we were able to compare the erythrocytes arrangement patterns in the retinal capillaries against what has also been described by Guevara-Torres et al, e.g., the parachute, zigzag, and disordered configuration [28]. High speed imaging revealed the erythrocyte velocity variation due to interaction with leukocytes (Figs. 9(a) and 9(b)) and temporal erythrocyte stasis due to non-linear flow at the confluent branching points (Fig. 9(c)) or local resistance (Fig. 9(d)). While these phenomena have been reported previously, we have observed different characteristics; we found that the arresting of the erythrocytes lasted approximately 0.25 second only. In contrast, Guevara-Torres et al reported that the erythrocyte flow stasis lasted from seconds to minutes in anesthetized mouse eye [28]. Flower and associates observed that numerous erythrocytes could pause for up to 20 seconds in monkey perifoveal capillaries and in the subfoveal choriocapillaris, and they also noted that individual erythrocytes could stop for 6 seconds in the rabbits' choriocapillaries [25]. Other studies also reported retinal capillaries flow stasis that lasted a few minutes due to leukocyte stops in monkey eyes [80] and in mouse eyes [81]. However, this phenomenon was not seen in cat eyes, either by direct imaging of unstained erythrocytes using white light gradient index of refraction lens endoscopy [82] or by imaging of fluorescent-tagged leukocytes [83]. Interestingly, studies in human eyes with normal health have not observed flow arresting [38]. However, these seem to be rare events and may be difficult to observe without larger data sets. Questions whether the flow stasis observed in animal eyes represents a natural event or artificial behavior of the cells caused by exogenous contrast agents [82] and whether this phenomenon can be used to assess pathophysiological condition of the blood cells as well as the retina remain to be investigated. Our instrument can image the erythrocyte flow in the living retina, noninvasively, with NIR light without affecting normal physiology of the retinal tissue and the retinal blood supply. Thus, it may help answer these questions through further study in more human eyes.

We acknowledge a fact that the quality of our image is not comparable to that acquired in anesthetized mouse eye using the AOSLO with split detection, as presented by Guevara-Torres et al [28]. They stopped the slow scanner of the AOSLO and projected a high frequency scanning light line on the capillary that was orthogonal to the scanning direction. In this way they generated a 1-D spatiotemporal image of individual blood cells. The image formed by multiply scattered light rendered the blood cells and the capillary wall with excellent contrast and specificity of cell types [28, 46, 52]. On the other hand, the method had its own limitations. It could only image the blood cells in the capillaries orthogonal to or having large angle with the fast line scan direction, and could image a single vessel only at a time. Moreover, their approach required a stabilized eye obtainable under anesthesia that would be challenging in the living human eye due to continuous eye movements with ocular pulse and micro-saccades even when fixating. Our approach using 2-D imaging can measure multiple vessels at a time, overcoming these limitations and thus can be used for living human patients.

4.5 Comparison with blood velocity and pulsatility reported in previous studies

Overall, the lower-bound values of the blood velocity and pulsatility range measured in this study agree well with previous publications; but the upper-bounds and the mean values are

Biomedical Optics EXPRESS

slightly higher (Table 4). However, if we constrain our measurement in capillaries containing well-separated singe file erythrocyte flow (whose spatiotemporal traces are in the form of the type 2 plot shown in Fig. 3(b)) only, the range and the mean of the velocity of this study become very well agree to those in published studies that measured on erythrocytes [46, 53]. Thus, the higher velocity and pulsatility were from the capillaries that contained densely packed erythrocytes. Another salient feature is that the velocity and the pulsatility measured in this study are higher than those reported on leukocytes. Tam reported a pulsatility index of 0.54 and 0.61 for leukocytes and plasma gaps in one eye of a normal subject [38]. Martin and Roorda found a leukocyte pulsatility index of 0.45 ± 0.09 [36]. Interestingly, the mean pulsatility index of our measurement is close to a blue-field entoptic study that reported a mean of 0.98 and a range between 0.80 and 1.17 in 5 subjects [84]. However, we should recognize that the entoptic phenomenon is thought to be based upon the perception of the leukocytes and it is unknown what size vessels correspond with the psychophysical and subjective measurement. In general, we expect that erythrocytes would move faster than leukocytes due to their smaller size and the small cross-sectional area of the capillaries [46, 83].

4.6 Importance of the measurement of continuous erythrocyte velocity waveform in the retinal capillary network

The cardiac-dependent pulsation of the blood flow has been well recognized in human retinal arterioles [44, 45] and in precapillary arterioles of the human conjunctiva [85], but it was only recently that the pulsatile movement of the erythrocytes was observed in human retinal capillaries [46]. Our study confirmed this important finding by measurement in more capillaries and more subjects.

Cardiac-dependent pulsation is an important character of blood circulation [86, 87]. Pulsatile movement of erythrocytes is essential for efficient oxygen transfer in pulmonary capillaries and is critical for brain capillary function and neural tissue health [86–89]. Disruption and loss of pulsatility may reduce circulation efficiency and cause tissue damage [86, 87, 90]. The continuous and high temporal resolution velocity waveform generated by the high speed and high-resolution imaging provided a fine measurement of the dynamic process of the pulsatile movement of the erythrocytes. Thus, this ability has the potential to identify new biomarkers for characterization of the capillary hemodynamics under normal physiological state, thereby laying a foundation for studies of altered retinal capillary blood flow under pathological conditions.

As presented in this study, the time of the erythrocyte velocity being accelerated from the diastolic state (V_{min}) to the systolic (V_{max}) and the raising rate of the velocity may bear estimations of the physical state of the capillaries. Longer time for cells to reach peak velocity in one cardiac cycle may indicate that the capillary has higher rigidness that increases the friction between the cell and the capillary wall, thereby delaying the time to reach the maximum velocity. Likewise, increased stiffness may increase the rising rate. We expect these parameters may be useful for the evaluation of aging effect and pathological condition of individual capillaries and microvascular networks. When applied to clinic studies, these metrics may contribute new information regarding the role of microvascular dysfunction in a variety of retinal and CNS diseases, as well as systemic conditions.

4.7 Importance of achieving long recordings of erythrocyte motion

Microcirculatory dysfunction has been implicated in a wide variety of pathologies in the retina and the CNS [4–11], either as a marker or as a mechanism. Many of these diseases, like diabetic retinopathy, are believed to originate first with capillary level changes. In Alzheimer's disease, cognitive decline and dementia have been found to be associated with disruption of blood flow in small cerebral vessels [90], and a recent study suggests that blood flow abnormalities may precede the neurodegeneration [11]. As a part of the CNS, the retina

Biomedical Optics EXPRESS

provides a unique window or sample for non-invasive assessment of the microcirculation of the CNS. The critical exchange of oxygen and metabolic byproducts is ultimately implemented by the erythrocytes in the retinal capillaries and mediated by retinal hemodynamic response system. Thus, precise characterization of the microcirculation dynamics in retinal capillaries using the erythrocytes as a surrogate may enable the investigation of potentially pathogenic flow at the most critical and vulnerable site, thereby providing early detection of the disease onset and prediction of disease progression. While animal models have provided important knowledge into mechanisms of microcirculation in health and disease, the human microcirculation has its own unique aspects that warrant investigation [91]. Therefore, knowledge of the mechanisms underlying the pathophysiology of retinal microcirculation obtained directly from the human patients is of fundamental clinical importance. To achieve this goal, noninvasive and accurate examination in the living human patient's eye over time without safety concern is critical. The high speed measurement of erythrocyte motion in retinal capillaries in this study was achieved by use of a NIR light source, which allows for long recording periods without initiating a phototoxic result in the retina. This ability may confer far-reaching benefits to basic vision science and clinical research on ocular, and systemic disorders. The approach described in this study may potentially facilitate development of novel treatment strategies by providing sensitive and precise assessment of the retinal hemodynamics before structural changes arise in the retinal vascular network.

4.8 Limitations and future improvements

First, the method presented in this study can accurately measure blood velocity in retinal capillaries (the 4th and 5th order vessels) whose diameters are smaller than 10 μm. We have estimated the measurement accuracy in blood vessels with diameter > 10 μm, but the test was limited by the frame rates. Thus, measurement accuracy in large vessels (diameter > 10 μm) remains to be determined. Accurate measurement of the blood velocity in large vessels may be achieved by the 1-D scanning strategy introduced by Zhong and associates [44]. This mechanism can be implemented in our instrument by stopping the field scanner on the selected vessels. Second, due to small field of view, the data analysis is time consuming as it has not been fully optimized. Thus, the results presented in this work were only acquired from a small number of healthy subjects. Future work will be focusing on enlarging the imaging field of view and developing fully automatic processing software. Furthermore, the measurement will be performed in additional subjects with stratified age ranges under well-controlled physiological conditions. Third, although the large majority of capillaries imaged in these subjects could be measured (92%), there were some of them that could not be measured due to insufficient clarity of the spatiotemporal traces of erythrocytes. This often happened with capillaries that were not within the central part of the imaging field. By reimaging these vessels in the center of the imaging frame, we were able to measure the velocity in these capillaries. We have recognized that this problem may be caused by the anamorphic illumination (formed by a cylindrical lens), especially when the AO adjusted light focal plane and added defocus to the deformable mirror, the image on the side of the camera sensor was out of focus. We are working on improved illumination strategies to overcome this problem. Fourth, although we have confirmed that the fluctuations in capillary flow are strongly related to the cardiac cycle, other factors such as respiration, intraocular pressure, which may affect the measurement remain to be investigated. In future study, we will assess the effect of these factors on erythrocyte motion in retinal capillaries. Finally, we feel it is necessary to point out certain caveats for the interpretation of the clusters of hypo- or hyper-reflective objects as leukocytes (depending on the focus layer), as shown in Figs. 2 and 9. While the model proposed by Uji et al and Arichika et al provided an excellent explanation of the observed phenomenon and there is good evidence to support their assumption is true [40, 41], there is not any yet definitive evidence that all of these events are leukocytes.

Biomedical Optics EXPRESS

Examples of cell aggregations, microthrombi, platelet clusters and other events may also impede the flow and cause the arresting events seen in our study. Thus, future investigations that can characterize the reflective or spectral properties of flowing particles as well as the clusters in the retinal capillaries are warranted. This finding can be critical for future pathological evaluations and useful for quantifying such events.

Despite the limitations, this study lays the foundation for investigating the retinal hemodynamics in the finest capillaries and microvascular networks using the erythrocytes as a surrogate in the living human eye. The continuous cardiac-dependent blood velocity waveform offers new avenue for looking into the dynamic property of the erythrocyte flow that is closely related to the physical state of the retinal capillary and its microvascular network, and to fundamental retinal physiology as well as pathophysiology. It is our hope that we can identify more sensitive and objective new biomarkers that may predict capillary structural changes associated with retinal pathology. Using the approaches described in this study, future studies will examine the hemodynamic metrics in the early and progressive stages of vascular disease in the retina. Accurate characterization of the hemodynamics in the retinal capillary may provide critical information on the evaluation of the efficacy of new interventional treatments for retinal vascular disease.

5. Conclusions

We demonstrated a method for *in vivo* direct measurement of erythrocyte dynamics in human retinal capillaries without visually evoked stimulation on the retina. This capability may facilitate new investigations on the pathophysiology of the retinal microcirculation with applications for ocular and systemic diseases.

Appendix 1: Quantification of blood flow velocity based upon the use of the Radon transform

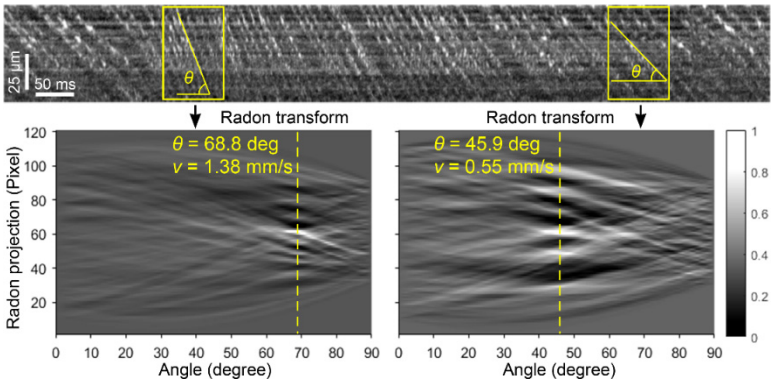

Fig. 12. Measuring the slope angle (i.e., the erythrocyte velocity) using the Radon transform. Top panel shows a spatiotemporal plot of the erythrocytes flow in a retinal capillary. Bottom panels present the Radon transform images of the spatiotemporal traces in the 2 yellow boxes. The angle corresponding to the maximum values (indicated by the yellow dashed lines) of the Radon transform represents an average measurement of the trace angle (the velocity) in the sampling window (yellow boxes).

Appendix 2: The merit function for optimizing the sampling window size

To measure the erythrocyte velocity, the slopes of the cell traces are measured along the time axis of the spatiotemporal plot, on n ($n = 1 - N$) sampling points. The velocity is measured within a sampling window, i.e., a piece of spatiotemporal image, with width of Δt. The Radon transform is performed on the sampled spatiotemporal image, generating a phase image $R(\rho,\theta)$. This process is actually computing the projection of the image in a series of the

Biomedical Optics EXPRESS

angular directions. The projection is the summation of the pixel intensities on every lines in a given angle θ, and ρ is the length of the projection.

First, we calculated the root mean square (RMS) for every angle of the phase image generated by Radon transform, assuming the size of phase image is $q \times p$, the RMS of a given angle θ_i is:

$$V(\theta_i) = \sqrt{\frac{1}{p}\sum_{j=1}^{p} R(\rho_j, \theta_i)^2}$$

At each velocity measuring point ($n = 1 - N$), we have a set of RMS $V(\theta_i) = \{V(\theta_1), V(\theta_2), \ldots V(\theta_q)\}$. We find the maximum value in $V(\theta_i)$ and normalize it with the RMS of entire phase image.

$$V_M(n) = \max_{1 \ll i \ll q}\{V(\theta_i)\} / \sqrt{\frac{1}{pq}\sum_{i=1}^{q}\sum_{j=1}^{p} R(\rho_j, \theta_i)^2}$$

where $V_M(n)$ is the normalized maximum RMS of the Radon transform at the n^{th} (velocity) measuring point. Over a total of N points, a sampling window with an optimal size (Δt) should generate a maximum mean value of the normalized maximum RMS at every measuring point.

$$M = \frac{1}{N}\sum_{n=1}^{N}\left\{\max_{1 \ll i \ll q}\left\{\sqrt{\frac{1}{p}\sum_{j=1}^{p} R(\rho_j, \theta_i)^2}\right\} / \sqrt{\frac{1}{pq}\sum_{i=1}^{q}\sum_{j=1}^{p} R(\rho_j, \theta_i)^2}\right\}_n$$

Funding

National Institutes of Health (EY024378 and P30 EY003039); the National Science Foundation (IIA-1539034); Intramural Research Program of the National Institutes of Health, National Eye Institute; Research to Prevent Blindness; EyeSight Foundation of Alabama; Buck Trust of Alabama.

Acknowledgments

We thank Austin Roorda PhD for advising the research and thank Jing Lu PhD for developing the adaptive optics near confocal ophthalmoscope.

Disclosures

BG, XW and CAG: University of Alabama at Birmingham (P); YZ: University of Alabama at Birmingham (P, F); MDT and JT declare no conflicts of interest related to this article.